Homeostatic regulation of M-current modulates synaptic integration in secretomotor, but not vasomotor, sympathetic neurons in the bullfrog

Paul H. M. Kullmann and John P. Horn

Department of Neurobiology and Center for Neuroscience, University of Pittsburgh School of Medicine, Pittsburgh, PA 15261, USA

We compared how vasomotor C neurons and secretomotor B neurons integrated identical patterns of virtual synaptic activity using dynamic clamp, perforated-patch recordings from dissociated bullfrog sympathetic ganglion cells. The synaptic template modelled one strong nicotinic synapse and nine weak synapses, each firing randomly at 5 Hz, with strength normalized to each cell. B neurons initially fired at 12 Hz, but this declined within seconds, decreasing 27% after 40 s and recovering slowly as evidenced by the threshold synaptic conductance for firing ($\tau_{recovery} = 136 \pm 23$ s). C neurons gave an identical initial response that remained steady, declining only 6% after 40 s. The difference resulted from an activity-dependent 379 ± 65% increase in M-current (I_M) in B cells ($\tau_{recovery} = 153 \pm 22$ s), which was absent in C cells. In addition, action potential afterhyperpolarizations were 2-fold longer in B cells, but this did not produce the differential response to synaptic stimulation. Activity-dependent increases in I_M were sensitive to 100 μM Cd^{2+} and 2.5 μM oxotremorine M (oxo-M), a muscarinic agonist, and fully blocked by zero Ca^{2+}, 10 μM oxo-M and 2.5 μM oxo-M plus 50 μM wortmannin, a PIP_2 synthesis inhibitor. A leftward shift in voltage-dependent activation could not fully account for the I_M increase. Firing at 0.5 Hz was sufficient to modulate I_M. Opposing influences of activity and muscarinic excitation thus produce homeostatic I_M regulation, to stabilize excitability and postsynaptic output in secretomotor sympathetic neurons. Absence of this regulation in vasomotor neurons suggests a different integrative function, where synaptic gain increases in proportion to presynaptic activity.

(Received 15 October 2009; accepted after revision 22 January 2010; first published online 25 January 2010)
Corresponding author J. P. Horn: Department of Neurobiology, E 1440 Starzl Biomedical Science Tower, University of Pittsburgh School of Medicine, Pittsburgh, PA 15261 USA. Email: jph@pitt.edu

Abbreviations AHP, afterhyperpolarization; gK_M, M-type K^+ conductance; g_{syn}, synaptic conductance; I_M, M-current; I_{M-30}, I_M at −30 mV; oxo-M, oxotremorine M; PIP_2, phosphatidylinositol-4,5-bisphosphate; threshold g_{syn}, threshold synaptic conductance; $V_{1/2}$, half-activation voltage.

Introduction

The M-type K^+ conductance (gK_M) mediated by KCNQ/K_V7 channels (Wang *et al.* 1998) was discovered in bullfrog sympathetic B neurons, where its muscarinic suppression gives a slow EPSP (Brown & Adams, 1980; Adams & Brown, 1982; Delmas & Brown, 2005). Excitatory muscarinic suppression of gK_M also operates in mammalian sympathetic neurons (Constanti & Brown, 1981; Brown & Selyanko, 1985; Marrion *et al.* 1987) and elsewhere, notably the hippocampus (Brown *et al.* 1990; Lawrence *et al.* 2006; Vervaeke *et al.* 2006; Shah *et al.* 2008) and cerebral cortex (Constanti & Galvan, 1983; Halliwell, 1986; McCormick & Prince, 1986). Muscarinic M_1 receptors and other metabotropic receptors suppress gK_M by interacting with $G_{q/11}$ to stimulate phospholipase Cβ and hydrolyse phosphatidylinositol-4,5-bisphosphate (PIP_2) (Suh & Hille, 2002; Ford *et al.* 2003; Zhang *et al.* 2003). Subsequent suppression of M-channel opening occurs through depletion of PIP_2 and, for some receptors (e.g. bradykinin), by elevation of cytoplasmic [Ca^{2+}] and its binding to calmodulin (Gamper & Shapiro, 2003; Winks *et al.* 2005; Suh *et al.* 2006; Hernandez *et al.* 2008*a*,*b*).

To understand how muscarinic excitation modulates the integration of fast nicotinic EPSPs in sympathetic ganglia, we have stimulated fully differentiated adult bullfrog sympathetic neurons in primary cell culture with complex patterns of virtual synaptic activity using the dynamic clamp method (Kullmann *et al.* 2004; Wheeler

 DOI: 10.1113/jphysiol.2009.182873

et al. 2004). With this approach one can functionally identify secretomotor B neurons and vasomotor C neurons by their different responses to muscarinic agonists (Kurenny *et al.* 1994) and then study their responses to stimulus patterns that reproduce synaptic activity observed *in vivo* (Ivanoff & Smith, 1995; McLachlan *et al.* 1997; McLachlan *et al.* 1998). Results from such experiments support the hypothesis that sympathetic ganglia act as amplifiers of presynaptic activity (Karila & Horn, 2000; Wheeler *et al.* 2004) and the prediction that postsynaptic muscarinic suppression of $g\mathrm{K_M}$ can enhance synaptic gain (Schobesberger *et al.* 2000; Kullmann & Horn, 2006). Other evidence indicating that physiological synaptic gain may actually triple sympathetic activity is provided by recent *in vivo* intracellular recordings from homologous vasomotor neurons in the rat, where two-thirds of postganglionic action potentials are reported to be driven by weak nicotinic synapses (Bratton *et al.* 2009). Nonetheless, an unexpected result of the earlier dynamic clamp experiments was the gradual decline of the B neuron response during sustained asynchronous barrages of virtual synaptic stimulation (Wheeler *et al.* 2004). It was therefore of interest to identify the conductance responsible for the reduction in excitability and to determine whether vasomotor C neurons exhibit similar activity-dependent behaviour.

Here we demonstrate two specializations in the intrinsic excitability of secretomotor B neurons and vasomotor C neurons. B and C type neurons differ in their spike after-potentials and in their susceptibility to activity-dependent change induced by physiologically realistic patterns of virtual synaptic activity. The responsiveness of B neurons declines during stimulation largely because of a Ca^{+2}-dependent shift in the voltage-dependent activation of $g\mathrm{K_M}$, an effect that can be elicited by very low, and physiologically relevant, firing frequencies. By contrast, this behaviour is absent in C neurons. These observations reveal that activity and muscarinic stimulation produce opposing postsynaptic effects on $g\mathrm{K_M}$, which may lead to the homeostatic stabilization of excitability in the secretomotor subpopulation of sympathetic neurons.

Methods

Cell culture

Experiments complied with local institutional guidelines, requirements set by the US National Institutes of Health, and *The Journal*'s policies and regulations (Drummond, 2009). Paravertebral sympathetic ganglia 9 and 10 were removed from adult bullfrogs (*Rana catesbeiana*, 5–7 inches, males and females) that had been killed by rapid spinal transection and double pithing using a procedure approved by the Institutional Animal Care and Use Committee at the University of Pittsburgh. After isolation, the ganglia were desheathed, cut into pieces, enzymatically digested using Liberase Blendzyme 3 (Roche Diagnostics, Indianapolis, IN, USA), mechanically dissociated, plated on glass coverslips coated with poly-D-lysine and maintained for up to 2 weeks (Wheeler *et al.* 2004). Under these conditions, process outgrowth in culture is minimal, with most neurons maintaining the normal monopolar shape found in the intact ganglion (Dodd & Horn, 1983).

Whole-cell recording, dynamic clamp and voltage clamp

We selected cells for recording that did not have processes. Perforated-patch recordings were made using heat-polished pipettes (2–4 MΩ resistance) filled with a solution containing amphotericin B (250 μg ml^{-1}) and (in mM) 110 potassium gluconate, 10 NaCl and 5 Na-Hepes, adjusted to pH 7.2. External Ringer solution contained (in mM) 115 NaCl, 2 KCl, 1.8 $CaCl_2$ and 4 Na-Hepes, adjusted to pH 7.4. Only recordings with access resistances $<$10 MΩ and resting potentials of at least $-$45 mV were accepted for analysis. B and C neurons were identified by their different muscarinic responses, which were assessed by measuring *I–V* relations under voltage clamp with slow voltage ramps (Kurenny *et al.* 1994). B neurons responded to oxotremorine M (oxo-M) with an inhibition of M-current, while C neurons responded with activation of a small inwardly rectifying K^+ current. Voltage clamp and dynamic clamp recordings were made with an Axoclamp 2B amplifier (Molecular Devices, Sunnyvale, CA, USA). The dynamic clamp system, which was operated at 20 kHz, consisted of an embedded computer running under a real-time operating system (National Instruments, Austin, TX, USA) and G-clamp software (http://hornlab.neurobio.pitt.edu) written in the LabVIEW-RT programming environment (Kullmann *et al.* 2004).

Virtual nicotinic synapses were implemented according to:

$$I_{\mathrm{syn}} = g_{\mathrm{syn}} \times (V_{\mathrm{M}} - E_{\mathrm{rev}})$$

with reversal potential (E_{rev}) set to 0 mV and synaptic conductance (g_{syn}) modelled as the sum of two exponentials having time constants of 1 ms (τ_{rise}) and 5 ms (τ_{fall}). A 40 s template mimicking the activity of one primary synapse and nine secondary synapses, each firing randomly at 5 Hz, was assembled by concatenating a noisy 4 s pattern 10 times (Wheeler *et al.* 2004). The 4 s pattern contained a total of 21 primary synaptic events and 187 subthreshold events, giving a mean rate of 5.2 Hz (((21 events + 187 events)/10 synapses)/4 s). We refer to this as the 40 s stimulus template. Gain elicited by the 40 s stimulus template was calculated, by counting the number

of spikes during each 4 s epoch and dividing the average postsynaptic firing rate by 5.2 Hz, the average presynaptic firing rate.

As in previous work, synaptic strength was normalized to threshold g_{syn}, the minimum virtual nicotinic conductance required to elicit an action potential in each neuron (Kullmann *et al.* 2004; Wheeler *et al.* 2004). After measuring threshold g_{syn} repeatedly to ascertain a stable baseline, we set the strength of the primary virtual synapse at 10 times threshold g_{syn} and secondary virtual synapses at 90% threshold g_{syn}. The 40 s stimulus template was then applied and afterwards, we resumed repeated measurements of threshold g_{syn} to monitor recovery and changes in the cell's condition.

M-current was measured under continuous single-electrode voltage clamp using one of two protocols, each starting at a holding potential of −30 mV where I_M is active. With the ramp protocol the holding potential was hyperpolarized at 20 mV s^{-1} until it reached −110 mV. The passive leak conductance of the cell was determined from the linear region of the *I–V* relation, typically between −60 to −80 mV, and leak subtracted current at −30 mV was taken as the measure of I_M. In the step protocol the holding potential was changed from −30 to −50 mV for 500 to 1000 ms.

I_M simulations employed a kinetic scheme (Yamada *et al.* 1989) describing the original M-current data from B neurons (Adams & Brown, 1982) with steady-state activation given by $1/(1+\exp(-(V-V_{1/2})/10))$ and the time constant by $1000/(3.3(\exp((V-V_{1/2})/40)+\exp(-(V-V_{1/2})/20)))$, where V is the membrane potential and $V_{1/2}$ is the half-activation voltage.

Statistical tests are identified in the text. The criterion for significance was $P < 0.05$. Summary data are expressed as the mean ± S.E.M.

Drugs and chemicals

Apamin, LY294002 and XE991 were purchased from Tocris (Ellisville, MO, USA). Amphotericin B, oxotremorine M, linopirdine, scyllatoxin, wortmannin and all other chemicals were from Sigma (St Louis, MO, USA).

Results

B and C neurons respond differently to an identical pattern of sustained synaptic stimulation

To determine whether the activity-dependent rundown of synaptic gain is a general property of all sympathetic neurons, B and C cells were identified by their different responses to oxo-M and then stimulated with an identical pattern of virtual nicotinic activity using the dynamic clamp. The synaptic command signal for the dynamic clamp was a 40 s conductance template containing strong and weak fast nicotinic events corresponding to the convergence of one strong synapse and nine weak synapses, all firing randomly at an average of 5.2 Hz. Although the time course of the synaptic conductance template was identical in all experiments, its amplitude was scaled to match the excitability of each cell by first measuring the threshold synaptic conductance (threshold g_{syn}), which is the minimum fast nicotinic conductance required to elicit a postsynaptic action potential (Kullmann *et al.* 2004). The strength of the synaptic template was then normalized by scaling the strong primary synapse to 10 times threshold g_{syn} and the weak secondary synapses to 90% of threshold g_{syn}. B cell templates were generally larger in amplitude than C cell templates because B cells have a higher threshold g_{syn} due to their larger size and lower intrinsic excitability (Kullmann & Horn, 2010). Since the temporal structure of the synaptic template was noisy by design, changes in the postsynaptic output during sustained stimulation could arise in part from statistical fluctuations of virtual synaptic activity. To minimize such effects, the 40 s stimulus template was constructed by repeating a random 4 s pattern 10 times and spike output was then analysed during each 4 s repeat.

The different responses of B and C cells to identical patterns of virtual synaptic stimulation took several seconds to develop (Fig. 1). During the initial 2 s of stimulation, the B cell in Fig. 1*A* and the C cell in Fig. 1*B* generated identical temporal patterns of 24 action potentials at an average rate of 12 Hz. Given the presynaptic firing rate of 5.2 Hz, this corresponds to a synaptic gain of 2.3. Comparing the synaptic conductance template (bottom traces in Fig. 1*A* and *B*) with the voltage recordings further reveals that 11 of the 24 action potentials during the first 2 s of stimulation were driven by strong primary EPSPs and the remaining 13 action potentials arose from summation between pairs of weak secondary EPSPs. Comparing the tenth repeat of stimulation with the first reveals an obvious decline in spike output by the B cell (Fig. 1*A*), but a more modest change in firing by the C cell (Fig. 1*B*). In this example, gain declined from an initial level of 2.3 to 1.6 in the B cell and from 2.3 to 2.1 in the C cell. As might be expected from the comparative weakness of secondary synapses, all of the spikes that dropped out of the pattern during sustained stimulation were events driven by summation of secondary EPSPs.

The effects of activity on spike output are also evident in plots of cumulative spike latency during entire 4 s repeats (Fig. 1*C–E*, same cells as in Fig. 1*A* and *B*). When the times of each spike during the first repeat are compared (Fig. 1*C*), the relations superimpose because the timing and number of spikes was nearly identical for the B cell and the C cell. Comparing spike latency during the first and

tenth repeats confirms that the decrease in spike output was greater in the B cell (Fig. 1*D*) than the C cell (Fig. 1*E*).

The activity-dependent decline in synaptic gain observed in individual neurons (Fig. 1*A* and *D*) was seen in 47 B cells (Fig. 1*F*) where gain decreased 27% from 2.17 ± 0.09 during the first 4 s of stimulation to 1.58 ± 0.05 during the tenth repeat. The grouped data also confirm that the onset of activity's effect on

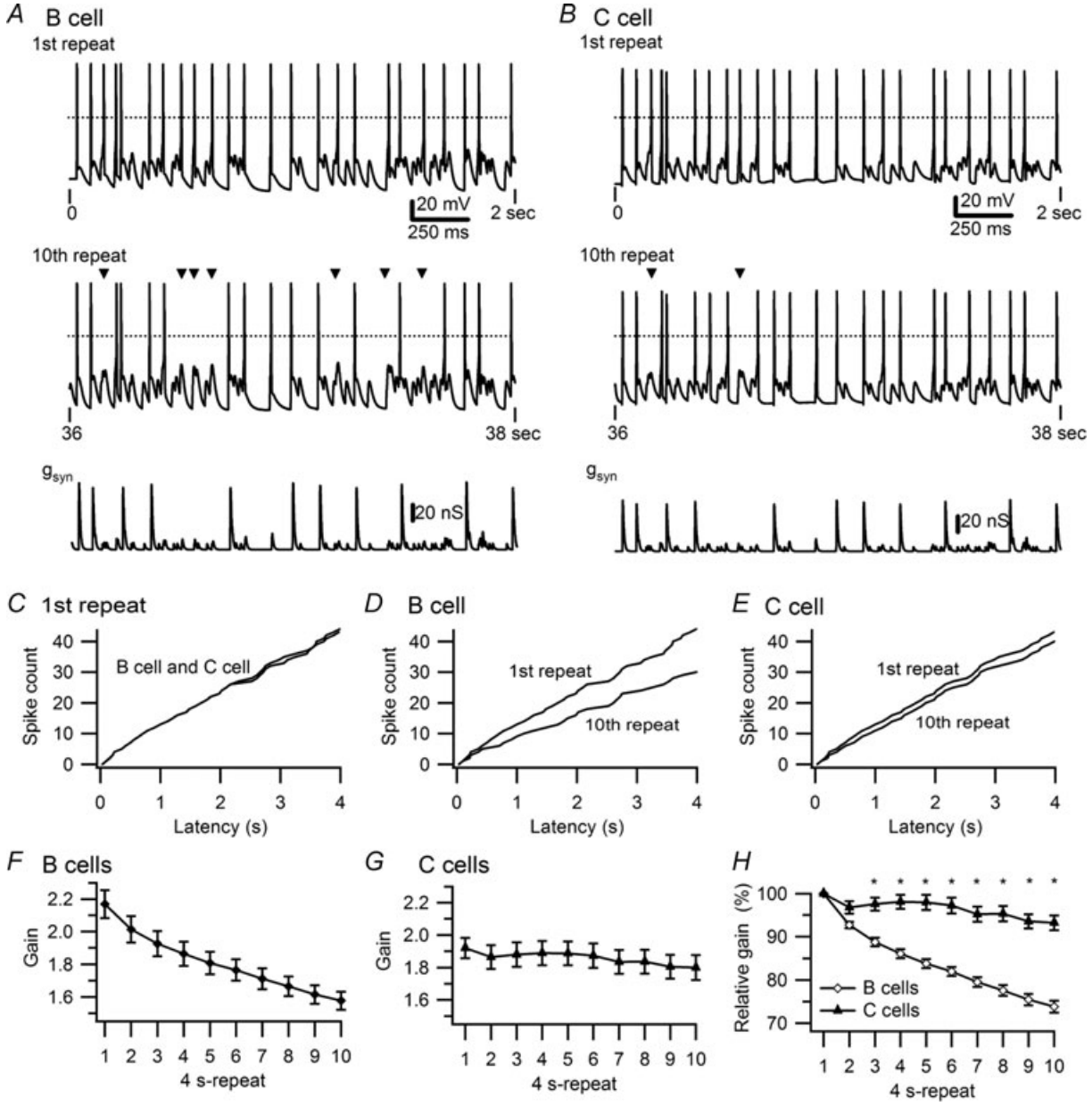

Figure 1. Differences in the activity dependence of synaptic gain in secretomotor B neurons and vasomotor C neurons

A and *B*, examples of responses in a B neuron and a C neuron to virtual synaptic stimulation using the 40 s, 5 Hz stimulus template that contained 10 repetitions of a 4 s pattern. Top traces show voltage recordings during the initial 2 s of stimulation. Dashed lines indicate 0 mV. Middle traces show responses to the same stimulus 36 s later during the 10th repeat of the pattern, with missing spikes marked by triangles. The amplitude of the conductance template (lower traces) used as the command signal for the dynamic clamp was larger in the B cell (*A*) than the C cell (*B*) because the B cell had a higher threshold g_{syn}. *C*, superimposition of cumulative latency plots of spikes during the first repeat (same cells as in *A* and *B*). Cumulative latencies of spikes during the first and 10th repeats show a larger decline in the B cell (*D*) than the C cell (*E*). *F*, plot of synaptic gain in 47 B neurons shows a 27% decline over 40 s of 5 Hz stimulation. *G*, plot of synaptic gain in 21 C neurons shows a 6% decline in response to identical stimulation. *H*, comparison of gain in B and C neurons, normalized to responses during the first stimulus repeat reveals that the difference becomes significant (*$P < 0.001$) by the third 4 s repeat.

gain was evident within seconds, becoming statistically significant by the second repeat in the template (1-way ANOVA, $P < 0.0001$). By contrast, the relative stability of synaptic gain illustrated by the C cell in Fig. 1*B* and *E* was representative of 23 C cells (Fig. 1*G*) where gain declined 6% from 1.94 ± 0.06 during the first 4 s repeat to 1.82 ± 0.08 during the last 4 s of stimulation. Although small, this decrease was significant for the seventh through tenth repeats (1-way ANOVA, $P < 0.0001$). The difference between B and C cells in the activity dependence of synaptic gain became significant by the third 4 s repeat (Fig. 1*H*) (2-way ANOVA, $P < 0.0001$). The average resting potential was -62.3 ± 1.2 mV in B cells and -63.4 ± 2.1 mV in C cells.

Variation in the action potential afterpotential does not account for cell specific differences in synaptic integration

The observation that Cd^{2+} enhances synaptic gain in B neurons (Wheeler *et al.* 2004) suggests that calcium entry during action potentials might serve to couple activity with the decreases in gain during virtual synaptic stimulation. To test this hypothesis, we first compared afterhyperpolarizations (AHPs) following action potentials elicited by one suprathreshold virtual nicotinic EPSP (Fig. 2*A*). Half-recovery time for the AHP in B cells was more than twice as long as in C cells (219 ± 10 ms, $n = 87$ *vs.* 93 ± 12 ms, $n = 31$; $P < 0.0001$, Mann–Whitney *U* test) and the peak AHP amplitude

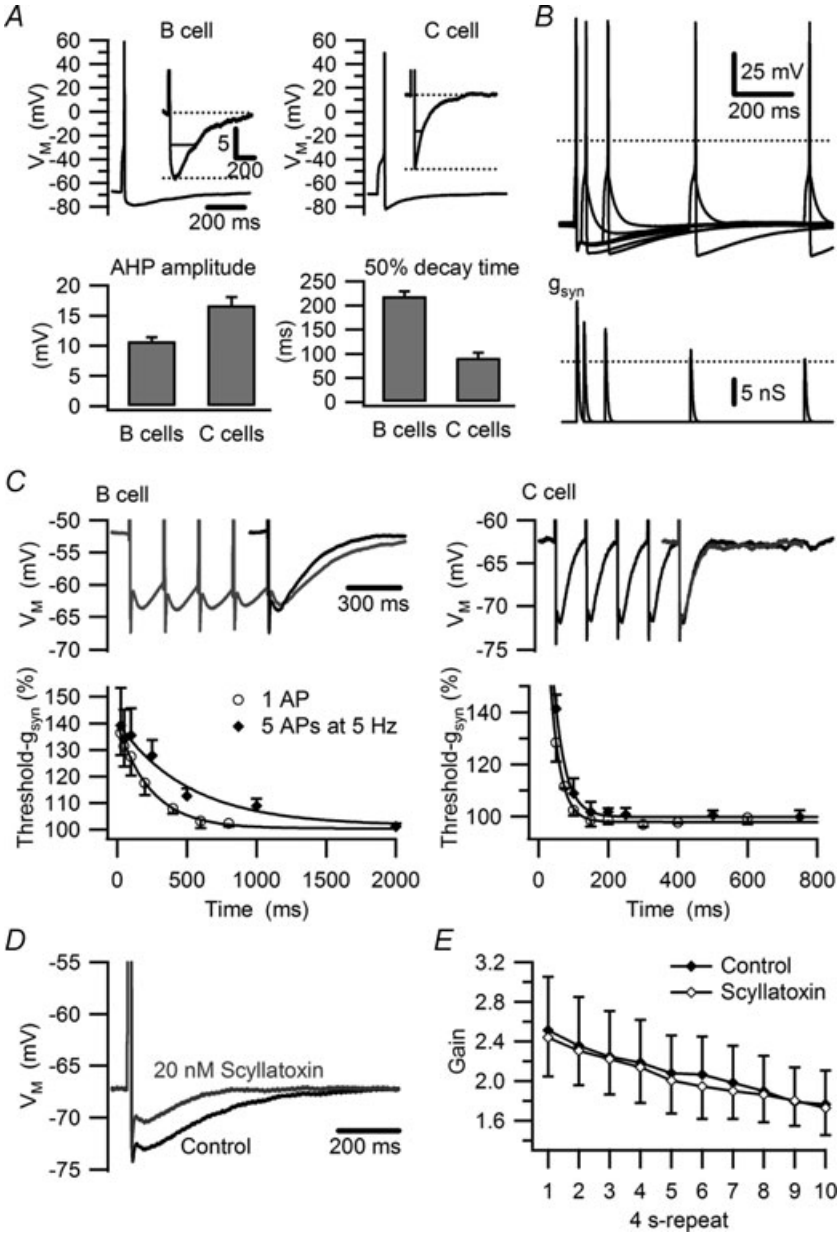

Figure 2. Phenotypic differences in the AHP do not account for differences in synaptic gain
A, comparison of B and C cells reveals a larger AHP amplitude in C cells and a longer AHP in B cells. Grouped data in bar graphs reflect 89 B cells and 33 C cells. *B*, method for measuring the time course of increased threshold g_{syn} during the AHP in a B neuron after a conditioning action potential elicited by a virtual nicotinic synapse set to twice threshold g_{syn}. Dotted lines denote 0 mV (upper panel) and the control value for threshold g_{syn} (lower panel). At each time point the voltage traces show one subthreshold and one suprathreshold response and the conductance traces show the corresponding threshold g_{syn}. *C*, comparison of AHPs elicited by single spikes and 5 spike trains (5 Hz) and the consequences for threshold g_{syn} in B neurons and C neurons. Single AHPs (black) are aligned with the last spike in the trains (grey). Summation of AHPs prolonged the transient increase of threshold g_{syn} in B neurons, but not in C neurons (see text for time constants derived from single exponential fits). *D*, 20 nM scyllatoxin blocks the AHP in a B neuron. *E*, plot of synaptic gain in B neurons showing that 20 nM scyllatoxin does not relieve the decrease in gain during 40 s, 5 Hz stimulation ($n = 4$).

was lower in B cells (Fig. 2*A*). Inhibition by the AHP was manifest as an increase in threshold g_{syn}, which was maximal near the peak of the AHP, and then decayed with a time course mirroring the AHP (Fig. 2*B*).

Following brief trains of 5 spikes at 5 Hz the AHP amplitude was unchanged, but AHP duration became slightly longer in B cells, but not in C cells (Fig. 2*C*). Increases in threshold g_{syn} also mirrored the time course of the AHP following five spike trains. Twenty-five milliseconds after a single action potential, threshold g_{syn} increased in B cells to $136.4 \pm 8.4\%$ of control ($n = 7$) and then recovered with a single exponential time constant of 242 ms (Fig. 2*C*). Following trains of five action potentials, the initial increase in threshold g_{syn} was no different than for a single spike ($139.2 \pm 14.0\%$ of control, $n = 5$, $P = 0.858$, *t* test), but the recovery time constant increased to 512 ms (Fig. 2*C*). This contrasted with C cells where the recovery time constant of threshold g_{syn} was much faster (29 ms) and unchanged by trains of five spikes (33 ms).

These observations support the idea that summation of the AHP produced by virtual synaptic activity at 5 Hz might cause the relatively large reduction of synaptic gain observed in B neurons. To test this possibility, the AHP was inhibited using 20 nM scyllatoxin, which blocks the SK-channels (Fig. 2*D*) that mediate the late component of the AHP (Kuba *et al.* 1983; Pennefather *et al.* 1985; Wei *et al.* 2005). However, this had no effect on the decline of synaptic gain during responses measured with the 40 s stimulus template ($n = 4$; $P > 0.05$, 2-way ANOVA; Fig. 2*E*). Identical results were obtained with 25–100 nM apamin, another SK-channel blocker ($n = 3$; not shown).

Increases in M-current parallel the decreased excitability evoked by synaptic stimulation

Earlier studies using stimulus protocols different from those employed here have shown that trains of action potentials increase intracellular $[Ca^{2+}]$ in B neurons and enhance M-current (I_M) (Marrion *et al.* 1991; Kirkwood & Lisman, 1992). To examine whether changes in gK_M could account for the activity dependence of synaptic gain, we studied the decrease in postsynaptic excitability immediately following sustained virtual synaptic stimulation. More specifically, we compared the time courses for changes in threshold g_{syn} and I_M using sequential trials under dynamic clamp and voltage clamp (Fig. 3*A*). This revealed a parallel time course for transient increases in threshold g_{syn} and I_M at -30 mV (I_{M-30}) (Fig. 3*A* inset). Following virtual synaptic stimulation with the 40 s template, threshold g_{syn} increased to $135.1 \pm 2.0\%$ of control ($n = 9$) and then slowly recovered over several minutes (Fig. 3*A*). Identical stimulation caused a transient increase of I_{M-30} to $379.2 \pm 65.4\%$ of control ($n = 20$; Fig. 3*D*). The time constants for recovery of I_{M-30} and threshold g_{syn} were indistinguishable ($\tau_{threshold,gsyn}$: 136 ± 23 s, $n = 9$; τI_{M-30}: 153 ± 22 s, $n = 20$; $P = 0.644$, *t* test; Fig. 3*B*). This contrasted with C cells where identical synaptic stimulation with the dynamic clamp elicited no change in I_{M-30} ($98.7 \pm 1.1\%$, $n = 7$; Fig. 3*C* and *D*). These experiments show that activity selectively enhances I_{M-30} in B neurons. This has the direct effect of dampening excitability, which reduces the effective strength of secondary nicotinic synapses (i.e. increased threshold g_{syn}) and thereby lowers synaptic gain.

Physiological levels of activity are sufficient to modulate I_M

The 5 Hz presynaptic firing rate and level of nicotinic convergence built into the dynamic clamp template were chosen to mimic realistic values in mammalian sympathetic ganglia and to facilitate the analysis by allowing more events to be collected in a 40 s trial (Wheeler *et al.* 2004). However, bullfrog B neurons receive only one or two secondary synaptic inputs (Karila & Horn, 2000) and they fire *in vivo* at rates on the order of 1 Hz (Ivanoff & Smith, 1995). To test whether the activity-dependent modulation of I_M also occurs under more physiological conditions, we elicited action potentials at constant rates of 0.5 and 1 Hz using 10 ms depolarizing current injections. These experiments did not investigate the effect of low frequency stimulation on threshold g_{syn} because the procedure for determining threshold g_{syn} can generate an action potential as often as every 2 s (0.5 Hz). Instead, cells were allowed to rest between repeated measurements of I_M at 5 min intervals. After establishing a baseline, low frequency stimulation was applied immediately after an I_M measurement, and then the I_M measurements resumed (Fig. 4*A*). One minute of stimulation at 0.5 Hz (30 action potentials) was sufficient to increase I_M. Doubling the number of action potentials during that period (1 Hz for 1 min) resulted in a slightly larger increase of I_M. Longer stimulation periods of up to 10 min further increased I_M while maintaining the frequency dependence (Fig. 4*B*). When cells were stimulated for two consecutive 5 min periods (Fig. 4*A*) the second 5 min period produced a much smaller increase in I_M than the first 5 min period. This suggests that the effect of constant stimulation saturates after about 10 min. Taken together, these experiments demonstrate that physiological levels of activity in bullfrog B neurons are sufficient to regulate basal I_M, while also allowing changes in activity to impose further influence upon I_M.

Oxotremorine-M and activity exert opposing effects on M-current and synaptic gain

We next examined whether virtual synaptic activity could overcome the suppression of I_M by a muscarinic agonist.

Measuring membrane current with 1 s voltage steps from −30 mV to −50 mV (Fig. 5) revealed that activity driven by the 40 s stimulus template caused a large increase in the slow current relaxations associated with M-channel closure during hyperpolarization and opening during depolarization. This was accompanied by a shift that more than doubled the holding current. Virtual synaptic stimulation continued to enhance I_M when gK_M was partially inhibited with 1 μM oxo-M, although not to the same extent observed in the absence of drug. During total inhibition of gK_M with 10 μM oxo-M, activity could no longer rescue I_M.

The effect of virtual synaptic activity on I_M in the presence of oxo-M was further studied using voltage ramps (Fig. 6). As seen with the voltage-step protocol, the 40 s stimulus template increased I_{M-30} during partial block of gK_M with 2.5 μM oxo-M (Fig. 6*A* and *C*), but the effect of activity on I_{M-30} disappeared in 10 μM oxo-M (Fig. 6*B* and *D*). Together, the observations with voltage-step and ramp protocols suggest that muscarinic receptors and activity modulate a common pool of channels and they imply that activity cannot overcome the PIP_2 requirement of M-channels, needed to maintain voltage-dependent gating.

If the activity-dependent increase of I_M causes the decrease in synaptic gain during prolonged stimulation (Fig. 1), then blocking M-channels with linopirdine or XE 991 should reduce or even prevent the decrease in gain. However, these drugs were ineffective. We found the drugs were unable to block gK_M in our current-clamp experiments because they acted in a voltage-dependent manner (not shown) and were ineffective at normal resting potentials, consistent with observations in mouse sympathetic neurons (Romero *et al.* 2004). As an alternative, we inhibited gK_M with oxo-M and analysed the consequences for synaptic gain. As expected from previous work (Kullmann & Horn, 2006), oxo-M increased synaptic gain by decreasing threshold g_{syn}. To separate this effect on excitability from the activity dependence of gain, we re-normalized the synaptic template after applying oxo-M to compensate the muscarinic reduction in threshold g_{syn}. As a consequence of this procedure, gain during the first

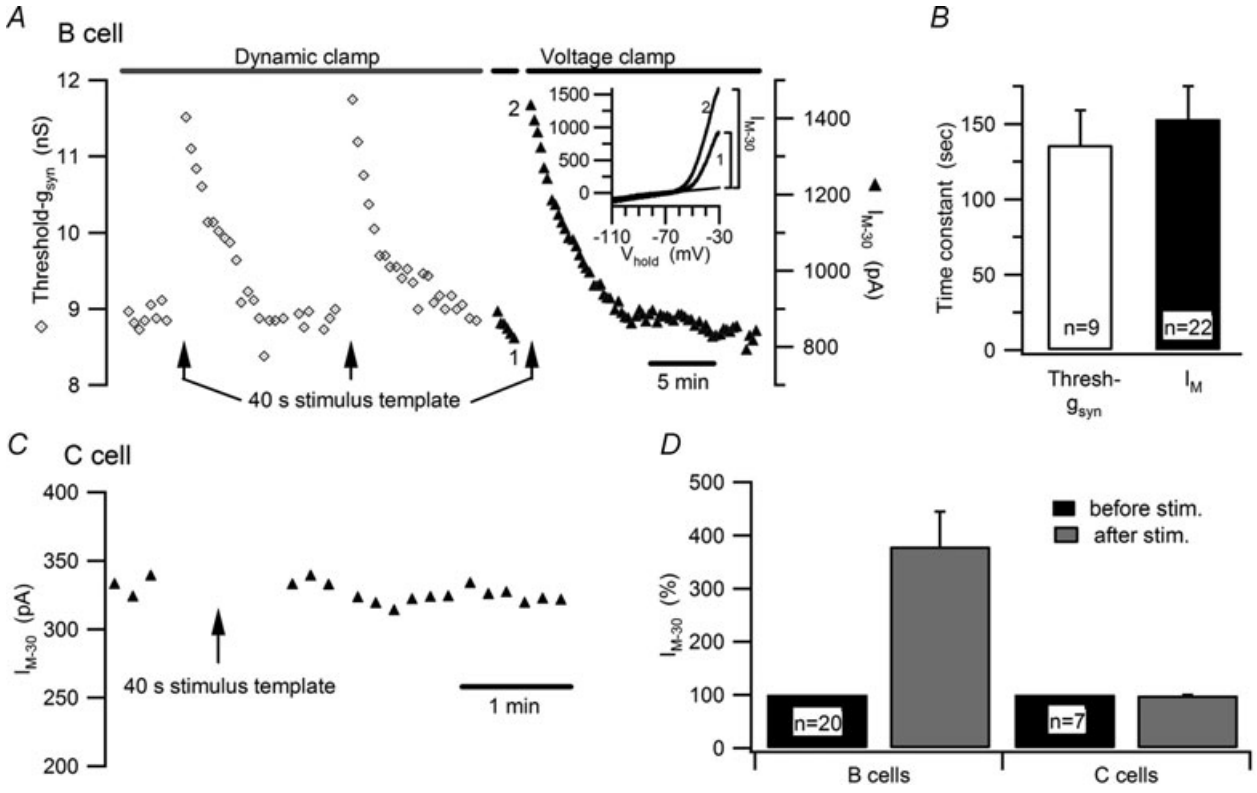

Figure 3. Virtual synaptic activity selectively enhances threshold g_{syn} and I_M in B neurons
A, time course of an experiment on a B neuron where the recording was switched between dynamic clamp and voltage clamp to measure the effects produced by the 40 s, 5 Hz stimulus template upon threshold g_{syn} (open diamonds) and I_{M-30} (filled triangles). *I–V* plots (inset) measured before (1) and after (2) stimulation illustrate the increase in I_{M-30} after leak subtraction. *B*, time constants for the recovery of threshold g_{syn} and I_M after 5 Hz stimulation were indistinguishable. *C*, time course of an experiment on a C neuron showing that activity elicited by the 40 s stimulus template under dynamic clamp had no effect on I_{M-30} measured under voltage clamp. *D*, grouped data showing that virtual synaptic stimulation selectively increases I_{M-30} in B neurons.

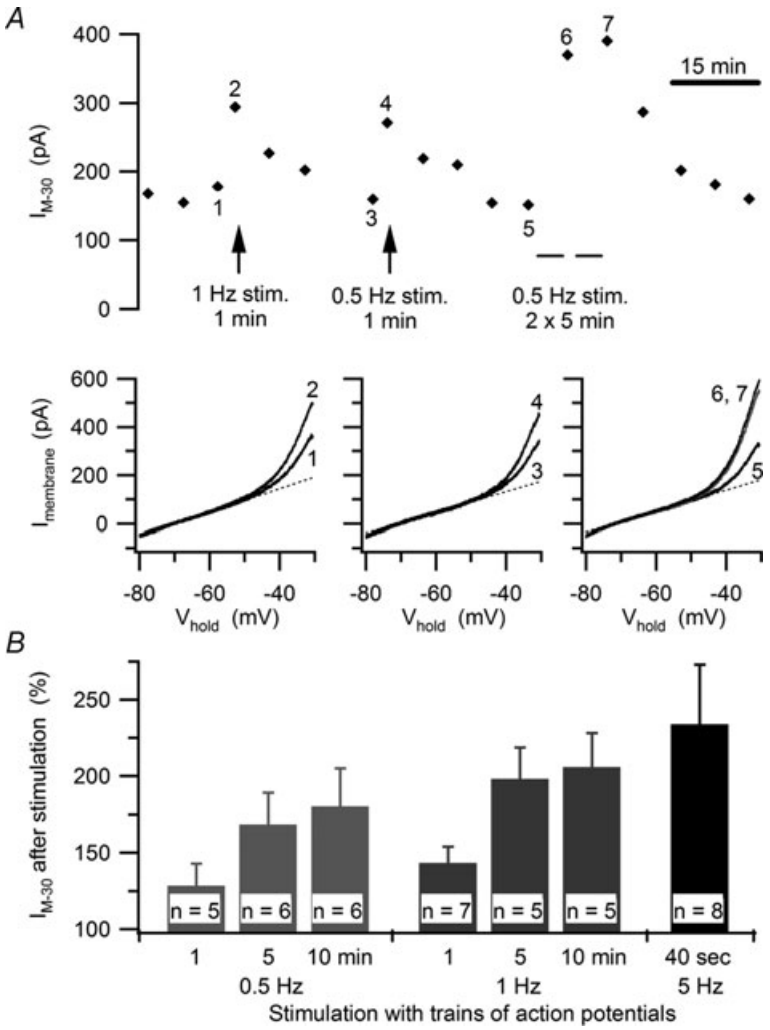

Figure 4. Physiological levels of activity enhance I_M in B neurons
A, time course of an experiment (upper panel) where increases in I_{M-30} were elicited by 1 Hz and 0.5 Hz trains of action potentials, which were stimulated with brief current pulses. *I–V* plots (lower panels) show the increases in I_M produced by each stimulus train. In each plot, the curves compare currents measured just before and just after stimulation, with numerals to show corresponding trials and dashed lines denoting the extrapolated leak currents. *B*, summary of experiments showing graded increases in I_{M-30} reflect the number and frequency of action potentials.

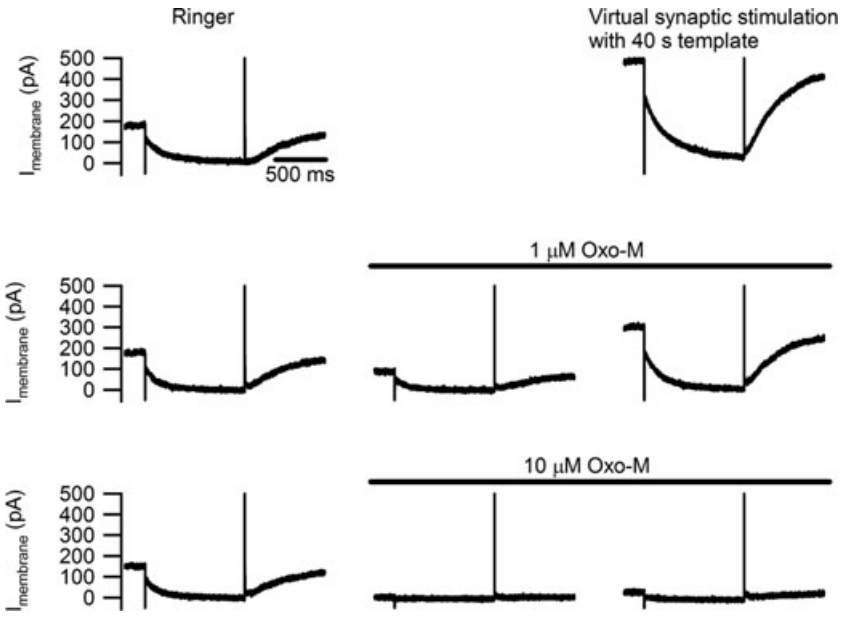

Figure 5. Activity enhances I_M during partial, but not complete, suppression by oxo-M
Currents recorded from a B neuron where I_M was measured by stepping from a holding potential of −30 mV to −50 mV. Top row shows the effect of activity produced by the 40 s, 5 Hz stimulus template in normal Ringer solution. Notice the increases in holding current and in the amplitudes of the slow current relaxations that reflect M channel gating. After the activity-induced increase in I_M subsided (middle row), 1 μM oxo-M inhibited I_M by about 50% and the 40 s stimulus template increased I_M beyond control levels. After washing out oxo-M and allowing the cell to recover from the previous stimulus trial (bottom row), I_M was completely suppressed by 10 μM oxo-M and under these conditions virtual synaptic stimulation failed to restore I_M.

4 s period of stimulation was the same in normal Ringer solution and in oxo-M (Fig. 6*E* and *F*). Although partial block of gK_M with 2.5 μM oxo-M had no discernable effect on the run-down of synaptic gain (2-way ANOVA, $P = 0.414$; Fig. 6*E*), full block with 10 μM oxo-M produced a clear reduction in the activity dependence of gain (2-way ANOVA, $P < 0.001$; Fig. 6*F*).

The effect of activity depends on Ca^{2+} and PIP_2

We were led to the hypothesis that Ca^{2+} links activity with the regulation of synaptic gain by evidence that 10 μM Cd^{2+} (Wheeler *et al.* 2004) enhances synaptic gain in B cells and that raising intracellular [Ca^{2+}] can increase I_M (Marrion *et al.* 1991; Yu *et al.* 1994). To confirm the link between activity-dependent Ca^{2+} influx and increased I_M, B neurons were stimulated with 40 s trains of action potentials delivered at 10 Hz using brief depolarizing current injections. This stimulus was chosen to deliver a constant number of action potentials at a frequency similar to that evoked by the 40 s, 5 Hz virtual synaptic protocol. The *I–V* curves in Fig. 7*A* illustrate a cell where 100 μM Cd^{2+} had little effect upon the resting I_M, but attenuated the effect of activity. This concentration of Cd^{2+} should block most voltage-dependent Ca^{2+} current into B neurons (Jones & Marks, 1989). Then, after treatment with 2.5 μM oxo-M the ability of activity to increase the remaining M-current (Fig. 7*A*) was further reduced by Cd^{2+}. Similar behaviour in four cells (Fig. 7*B*) confirmed that action potentials increase I_M, that this mechanism persists during submaximal muscarinic excitation, and that it is Cd^{2+} sensitive.

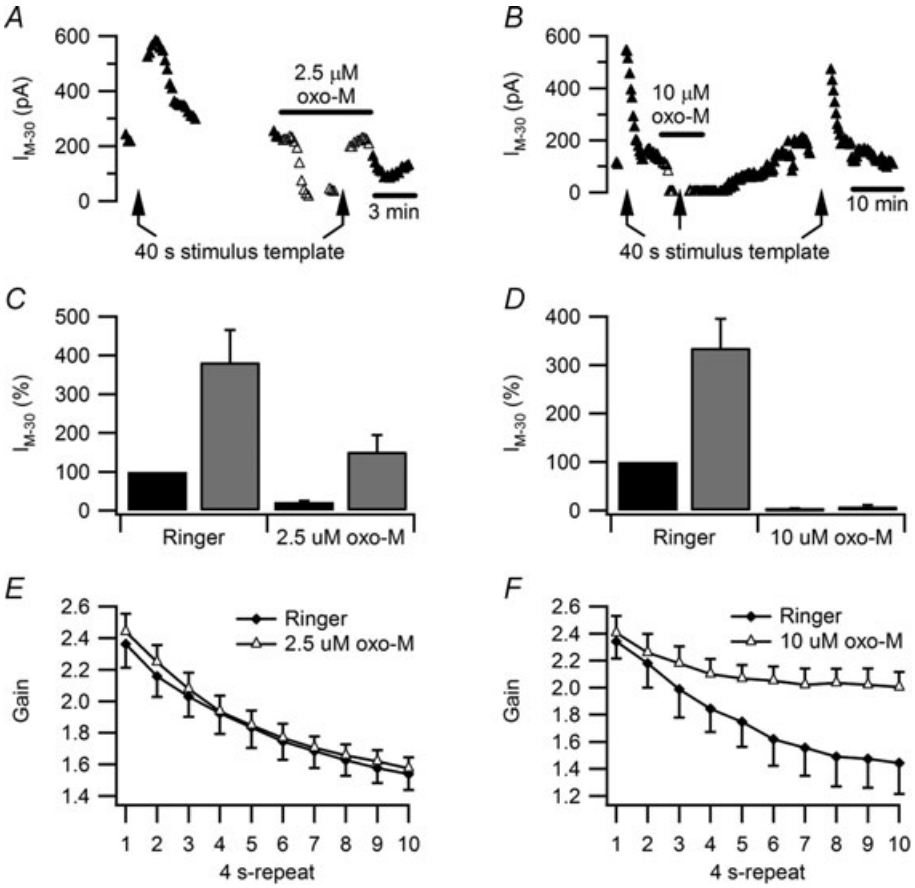

Figure 6. Complete suppression of I_M by oxo-M occludes the effect of activity upon synaptic gain
A and *B*, time courses of two experiments in which slow voltage ramps were used to monitor the effects of stimulation with the 40 s, 5 Hz template on I_{M-30} in normal Ringer solution and oxo-M. During partial inhibition of I_M by 2.5 μM oxo-M (*A*) activity increased I_{M-30} with a time course similar to that seen in normal Ringer solution. During complete inhibition of I_M by 10 μM oxo-M (*B*) activity failed to enhance I_{M-30}. *C*, data from 12 neurons showing the effect of activity persists during partial I_M inhibition with 2.5 μM oxo-M. *D*, data from 4 neurons showing 10 μM oxo-M occludes the effect of activity on I_{M-30}. *E*, plots of synaptic gain show no difference between normal Ringer solution and 2.5 μM oxo-M. For these comparisons the synaptic template was rescaled in oxo-M to compensate for the muscarinic increase in excitability. *F*, similar plots comparing control Ringer solution with 10 μM oxo-M show that complete suppression of I_M prevents most of the activity-dependent decline in synaptic gain.

We have already argued that PIP_2 plays a permissive role in the enhancement of I_M by activity, based on the loss of this regulation during maximal muscarinic stimulation with 10 μM oxo-M (Figs 5 and 6). A second strategy for testing this idea was to deplete PIP_2 by stimulating phospholipase C activity with a submaximal dose of oxo-M, while also blocking PIP_2 synthesis using wortmannin, a phosphoinositide 4-kinase inhibitor. In 5 of 5 cells treated with 2.5 μM oxo-M and stimulated with 40 s, 10 Hz spike trains, wortmannin either reduced (10 μM, $n = 2$; Fig. 7*C* and *E*) or blocked (50 μM, $n = 3$; Fig. 7*D* and *E*) the activity-dependent increase in I_M. To control for inhibition of phosphoinositide 3-kinase by wortmannin, we tested a specific PI3-kinase inhibitor. LY294002 (10 μM) had no effect on the spike induced enhancement of I_M in normal Ringer solution ($n = 6$) or in the presence of 2.5 μM oxo-M ($n = 4$; not shown).

To provide a more direct test that modulation of M-current by activity requires Ca^{2+} entry, while also controlling for possible non-specific effects of Cd^{2+}, we next replaced extracellular Ca^{2+} with 1.8 mM Mg^{2+} plus 100 μM EGTA. In zero extracellular Ca^{2+}, the enhancement of I_M by virtual synaptic stimulation with the 40 s template was completely inhibited (Fig. 8*A*) in 6 of 6 B neurons (Fig. 8*B*). Zero Ca^{2+} also inhibited the activity-dependent decrease in synaptic gain elicited by the 40 s stimulus template (Fig. 8*C*). The effect of Ca^{2+} removal thus appeared very similar to that when I_M

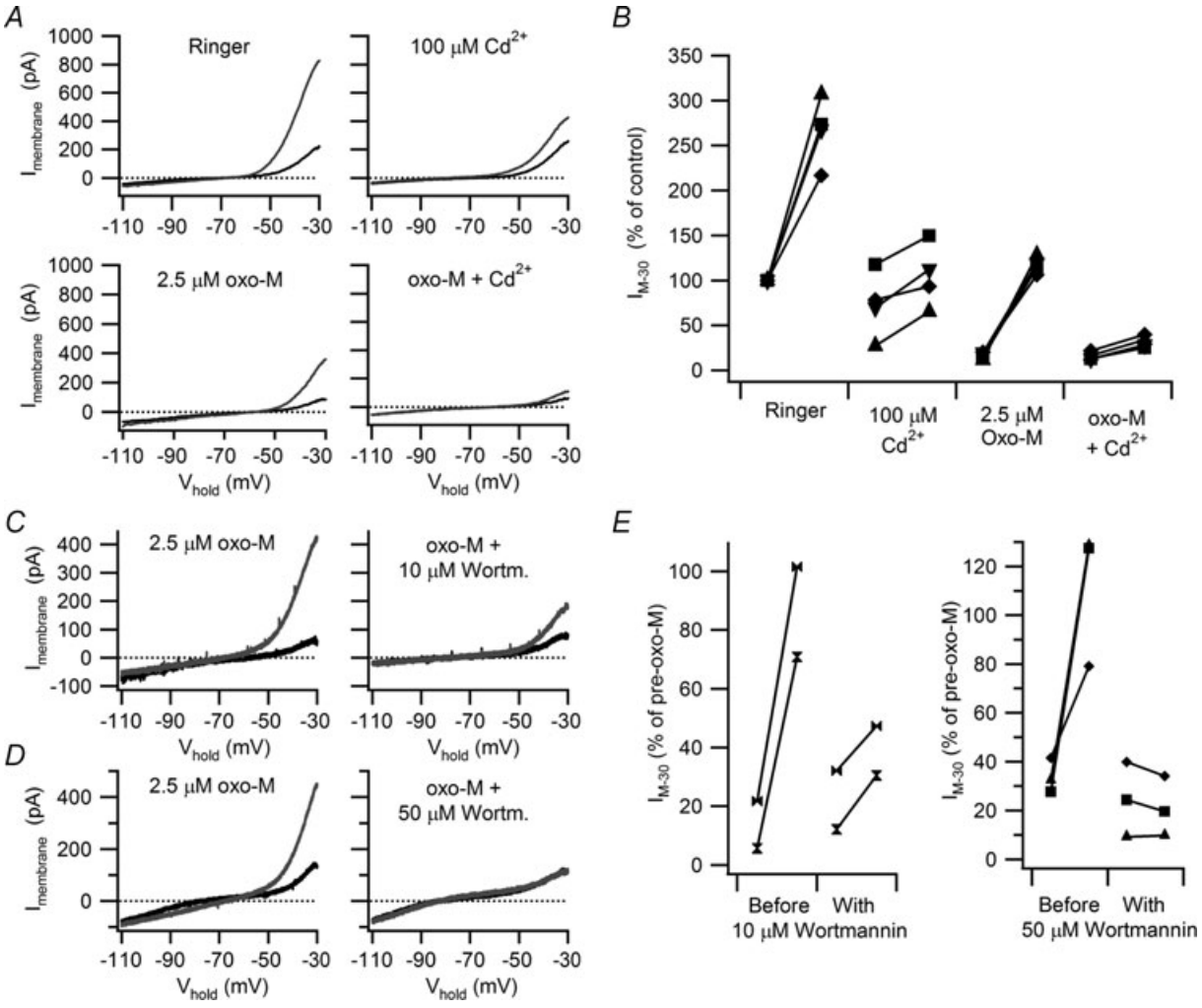

Figure 7. Cd^{2+} and wortmannin inhibit the activity-dependent enhancement of I_M
A, *I–V* relations from an experiment on a B neuron where the increase in I_M produced by a 40 s, 10 Hz train of action potentials was attenuated by 100 μM Cd^{2+} and almost entirely eliminated after partial I_M suppression with 2.5 μM oxo-M. *B*, data from four cells that all behaved like the cell in panel *A*. In these plots, I_M was normalized to the resting level in Ringer solution prior to any stimulation. *C* and *D*, *I–V* relations illustrating how the effect of 40 s, 10 Hz train of action potentials was reduced in 10 μM wortmannin (*C*) and elimated in 50 μM wortmannin (*D*) in cells where I_M had been partially suppressed with 2.5 μM oxo-M. *E*, similar effects of oxo-M plus wortmannin were observed in 5 of 5 neurons where activity-dependent increases in I_M were reduced or eliminated.

was completely inhibited by 10 μM oxo-M and no longer enhanced by activity (Fig. 6*B*, *D* and *F*).

Activity enhances I_M by shifting its voltage dependence

In principle, activity could enhance I_M through an increase in conductance or by a hyperpolarizing shift in its voltage-dependent gating. To distinguish these possibilities, *I–V* curves were measured in control Ringer solution, before and after virtual synaptic stimulation (Fig. 9*A*) and then leak subtracted to produce *I–V* relations that reflect I_M (Fig. 9*B*). This approach relies on the fact that in B neurons the *I–V* relation is dominated by a linear leak conductance between −90 and −70 mV and by gK_M between −60 and −30 mV (Adams *et al.* 1982*a*). To compare the smaller current measured before stimulation with the larger current measured afterwards, the former was scaled so that the two currents matched at −30 mV (Fig. 9*B*). This revealed that the current measured after stimulation activated at more negative membrane potentials. A similar leftward shift was observed in 12 of 13 cells. This implies that activity enhances I_M by shifting the gK_M activation curve in the hyperpolarizing direction.

The same analysis was also performed with *I–V* data measured in control Ringer solution and in oxo-M (Fig. 9*C* and *D*). After leak subtraction and scaling, the smaller M-currents measured in oxo-M superimposed with control currents (Fig. 9*D*) in 6 of 7 cells. This conforms with the evidence that muscarinic suppression of I_M arises from hydrolysis of PIP_2 and a loss of gating in channels that become quiescent, without any shift in the voltage dependence of remaining channels (Adams *et al.* 1982*b*; Suh *et al.* 2004; Delmas & Brown, 2005; Hernandez *et al.* 2008*b*).

To provide a further test of the analysis, M-currents were simulated using a standard kinetic model of the conductance in conjunction with our dynamic clamp system (Yamada *et al.* 1989; Schobesberger *et al.* 2000; Kullmann *et al.* 2004). For this purpose, we plotted simulated M-currents for total conductances of 40 nS and 80 nS with a half-activation voltage ($V_{1/2}$) of −35 mV and for 40 nS with $V_{1/2} = -20$ mV (Fig. 9*E*). When the two currents with the same $V_{1/2}$ were scaled, they superimposed (Fig. 9*F*). However, upon scaling the smaller current with $V_{1/2} = -20$ mV and comparing it with the curves where $V_{1/2} = -35$ mV, they did not superimpose, but instead resembled the comparison between resting control and activity enhanced M-currents (Fig. 9*B* and *F*).

Discussion

In this study, we used a standardized virtual synaptic stimulus to compare the integrative properties of identified secretomotor B neurons and vasomotor C neurons. Although the responses to synthetic synaptic activity were initially identical in both cell types, the post-synaptic firing generated in B cells began to decline after several seconds and this process persisted throughout 40 s of stimulation (Fig. 1). The design of the synaptic stimulus template in these dynamic clamp experiments was guided by a general theory that proposes synaptic integration

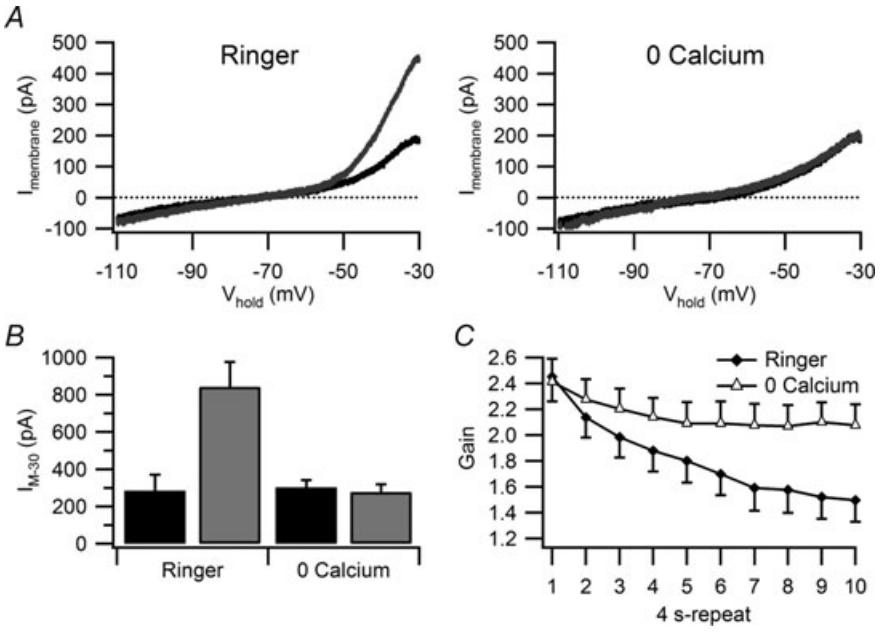

Figure 8. Removal of extracellular Ca^{2+} blocks the activity-dependent enhancement of I_M together with the activity-dependent decline in synaptic gain
A, replacement of extracellular Ca^{2+} with Mg^{2+} blocked changes in the *I–V* curves induced by stimulation with the 40 s synaptic template. Curves in black were recorded before stimulation and curves in grey after stimulation. *B*, similar results were seen in 6 of 6 B neurons where Ca^{2+} removal blocked the activity-dependent increase in I_{M-30} ($P = 0.0002$). *C*, gain measurements from the same 6 neurons showing that Ca^{2+} also inhibited the decline in gain normally seen during virtual synaptic stimulation. Differences between the two curves are significant by the fourth 4 s repeat ($P < 0.01$).

in paravertebral sympathetic ganglia serves to amplify preganglionic activity as a consequence of summation between weak secondary nicotinic fast EPSPs (Karila & Horn, 2000). Previous computational simulations of a conductance-based model B neuron failed to predict the activity dependence of synaptic gain seen in real B neurons (Wheeler *et al.* 2004). We suspected that limitations in the computational model stemmed from the omission of Ca^{2+} and Ca^{2+}-dependent regulation, which was done to avoid the numerous assumptions required to model these complex processes (Yamada *et al.* 1989). Instead of developing a more elaborate model, we conducted the present electrophysiology experiments in order to understand how B and C cells differ.

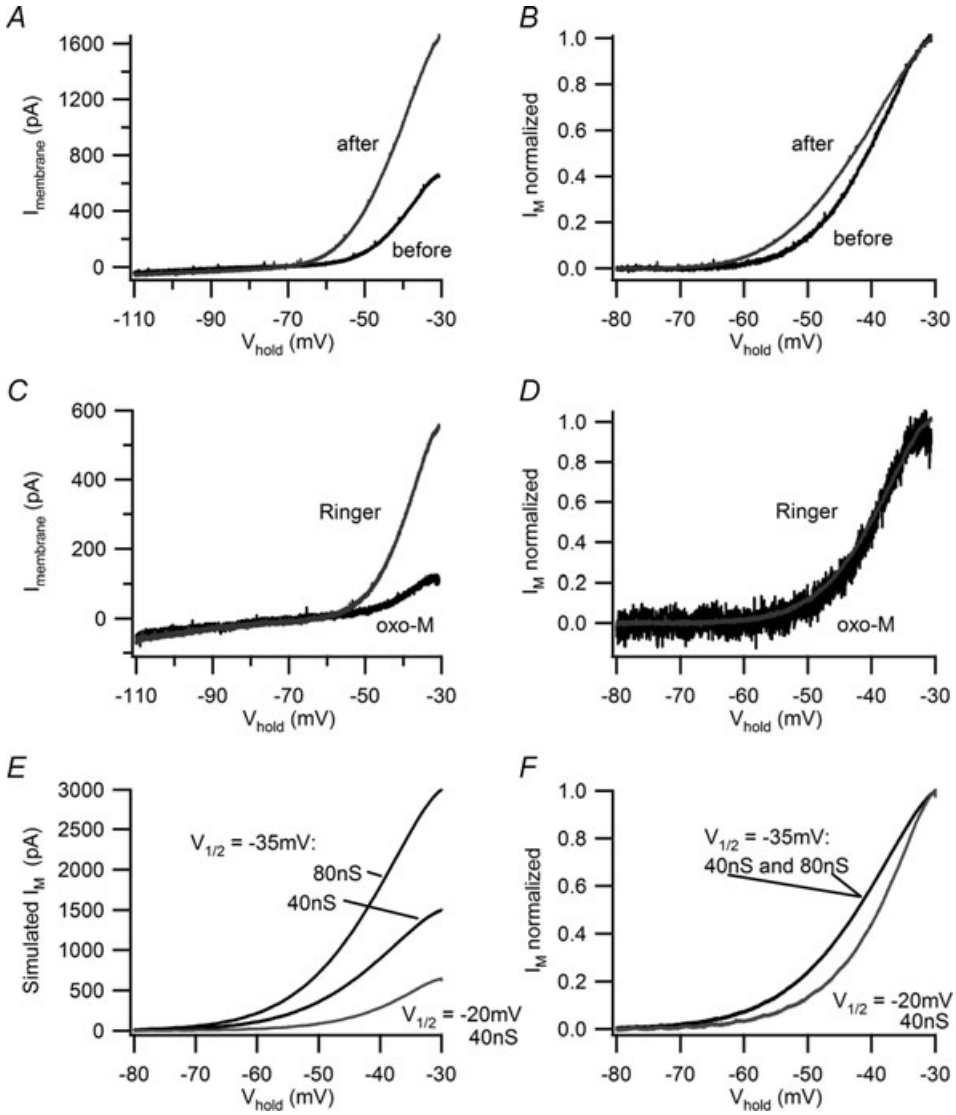

Figure 9. Activity shifts the voltage dependence of I_M
A, *I–V* plots measured with voltage ramps before (black) and after (grey) virtual synaptic stimulation with the 40 s, 5 Hz stimulus template show the typical increase induced by activity in B neurons. In this example, there was an approximate doubling of I_{M-30}. *B*, normalized *I–V* plots of I_M were constructed by leak subtracting the data in panel *A* and scaling the smaller 'before' current to match the 'after' current at −30 mV. This reveals that activity produced a hyperpolarizing shift in the *I–V* relation for I_M. *C* and *D*, conducting the same analysis for 2.5 μM oxo-M shows that it suppressed I_M in a resting B neuron by more than 50% (*C*) without altering its voltage dependence (*D*). *E* and *F*, simulating I_M with the standard biophysical model (see text for details) confirms the interpretation of B cell data. *E*, *I–V* plots for simulated I_M show one can double I_{M-30} either by doubling the maximal conductance from 40 nS to 80 nS or by shifting $V_{1/2}$ from −20 mV to −35 mV. *F*, upon normalizing the simulated M currents, the *I–V* relations superimpose for 40 nS and 80 nS with $V_{1/2} = -35$ mV and they are to the left of the current simulated with $V_{1/2} = -20$ mV. Shifting $V_{1/2}$ to the left thus reproduces the effect of activity (*B*) and simply lowering the maximal conductance replicates muscarinic excitation (*D*).

To test the hypothesis that Ca^{2+} entry through voltage-gated Ca^{2+} channels provides the critical link between activity and the regulation of excitability, we focused on the AHP and gK_M. Comparing action potentials revealed that the AHP was much longer in B cells than in C cells and that it underwent moderate summation in B cells (Fig. 2). In both cell types, the reduction in excitability during the AHP was evident as a transient increase in threshold g_{syn}, an effect that could in principle lower synaptic gain. However, blocking the AHP with scyllatoxin and apamin did not alter the activity dependence of gain in B cells. We conclude that the AHP can shape synaptic integration in sympathetic neurons, but does not account for the slow changes caused by sustained activity. B neurons also express a second Ca^{2+}-activated K^+ conductance mediated by large-conductance, TEA-sensitive C-type channels (Pennefather *et al.* 1985). Because the C-type K^+ current is fast and contributes primarily to action potential repolarization, it also seems unlikely as the mechanism for synaptic gain regulation by sustained activity.

Several lines of evidence support the conclusion that an activity-dependent increase in M-current was largely responsible for the activity-driven decline of synaptic gain in sympathetic B neurons. First, virtual synaptic stimulation with the 40 s, 5 Hz template led to a decrease in excitability that was manifest by increases in threshold g_{syn} and I_{M-30} (Fig. 3). Second, these two effects recovered with the same time course. Third, activity-dependent changes in I_M were absent in C neurons (Fig. 3*C* and *D*), where decreases in gain were very small (Fig. 1*D* and *E*). Fourth, complete suppression of I_M with 10 μM oxo-M reduced the activity-dependent decrease in gain to a level comparable to that seen in C neurons (Figs 1*E* and 6*F*).

Early studies of synaptic mechanisms in ganglia often employed high stimulus frequencies to evoke large responses that would be easier to detect. Previous studies showing that action potentials increase I_M in B neurons employed very intense stimulation (900 spikes at 30 Hz; Kirkwood & Lisman, 1992) or TEA to enhance action potential duration (Marrion *et al.* 1991). Our results extend these findings by showing that 5 Hz stimulation in physiological Ringer solution is more than sufficient to modulate I_M. More important, the ability of 0.5 Hz stimulation to modulate I_M (Fig. 4) shows that this mechanism can operate under conditions seen *in vivo* (Ivanoff & Smith, 1995).

The small activity-dependent gain decrease in C neurons and in B neurons treated with 10 μM oxo-M indicates that conductances other than gK_M can also be influenced by activity. We did not study these effects and the identities of the underlying conductances remain unknown.

Possible mechanisms for M-current regulation by activity

Evidence that voltage-dependent Ca^{2+} influx causes the activity-dependent increase in I_M is provided by its sensitivity to 100 μM Cd^{2+} (Fig. 7*A* and *B*) and to removal of extracellular Ca^{2+} (Fig. 8). This interpretation agrees with earlier experiments, which employed Ca^{2+} imaging, photolytic release of caged Ca^{2+} and intracellular dialysis of Ca^{2+} buffers to demonstrate that raising $[Ca^{2+}]_i$ from 0 to 120 nM doubled I_M (Marrion *et al.* 1991; Yu *et al.* 1994; Tokimasa *et al.* 1996; Tokimasa *et al.* 1997). Over a larger range $[Ca^{2+}]_i$ exerts a biphasic influence; 450 nM inhibits I_M in B neurons (Marrion *et al.* 1991; Yu *et al.* 1994). To our knowledge, there is no evidence for Ca^{2+}-dependent enhancement of I_M in rat sympathetic neurons.

Only recently has it become clear that M-channel gating requires PIP_2 and that depletion of PIP_2 by phospholipase C-mediated cleavage to form diacylglycerol and inositol trisphosphate (IP_3) provides the most common mechanism for suppression of M-current by $G_{q/11}$-coupled receptors in amphibian and mammalian neurons (Suh & Hille, 2002; Ford *et al.* 2003; Delmas & Brown, 2005; Suh *et al.* 2006). A second mechanism of I_M inhibition has been characterized in rat sympathetic neurons where calmodulin bound to the carboxy-terminus of KCNQ channels confers inhibitory calcium sensitivity to M-channels (Gamper & Shapiro, 2003). Thus, in rat sympathetic neurons muscarinic stimulation inhibits I_M via depletion of PIP_2 without affecting $[Ca^{2+}]_i$, while bradykinin inhibits I_M via IP_3-induced release of calcium from intracellular stores. At the same time the bradykinin-induced degradation of PIP_2 is compensated by enhanced re-synthesis of PIP_2 (Gamper & Shapiro, 2003; Delmas & Brown, 2005; Winks *et al.* 2005; Hernandez *et al.* 2008*a*).

Against this backdrop, how does activity increase I_M in B neurons? Perhaps the simplest explanation is that shifting the voltage dependence of M-channels (Fig. 9) allows for a greater fraction of M-channels to open at subthreshold membrane potentials. However, this explanation is insufficient for the following reasons. In previous voltage-clamp experiments where $[Ca^{2+}]_i$ was raised from near zero to $\geq$120 nM, this resulted in an approximate doubling of M-current and a shift in $V_{1/2}$ for gK_M from -20 mV to -40 mV (Yu *et al.* 1994; Tokimasa *et al.* 1996). Our data indicate a similar leftward shift in *I–V* relations for I_M (compare Fig. 9*B* with Fig. 9*F*). However, shifting $V_{1/2}$ by 15–20 mV can do little more than double the magnitude of I_{M-30} based on simulations (Fig. 9*E*) using the standard model for activation of gK_M (Yamada *et al.* 1989), even if one varies the slope of the activation curve and the magnitude of the shift in $V_{1/2}$. This is problematic because in many though not all of our perforated-patch recordings, activity induced

nearly fourfold increases in I_{M-30} (Figs 3*D*, 7*A*). The simplest way to account for the disparity between such large increases in I_{M-30} and the maximal effects of shifting $V_{1/2}$ is to invoke a second mechanism through which activity increases the number of functional M-channels. This might occur through an increase in membrane PIP_2 that unmasks quiescent M-channels. The plausibility of such a mechanism is supported by experiments on rat sympathetic neurons, where it is estimated that at rest only 70–80% of M-channels are functional (Suh *et al.* 2004; Winks *et al.* 2005). One way in which activity might cause a Ca^{2+}-dependent increase in PIP_2 abundance involves the neuronal calcium sensor-1 protein, a Ca^{2+} binding protein that stimulates PI-4 kinase activity and PIP_2 synthesis (Zhao *et al.* 2001; Gamper *et al.* 2004; Winks *et al.* 2005; Zaika *et al.* 2007).

Signalling through arachadonic acid may also play a key role in the Ca^{2+}-dependent regulation of M-channel gating in B neurons (Yu, 1995). Exogenous arachadonic acid mimics the effect of raising $[Ca^{2+}]_i$ upon the voltage sensitivity and magnitude of I_M and antagonists of phospholipase A_2 block these effects. These prescient observations merit further examination now that PIP_2's role in gK_M regulation has been discovered.

Implications for synaptic homeostasis and physiological autonomic homeostasis

Walter Cannon defined the concept of homeostasis to describe mechanisms that control and stabilize physiological parameters such as body temperature, blood pressure and serum electrolyte concentrations. Recently, homeostasis has been extended to molecular and biophysical mechanisms that stabilize neuronal excitability and synaptic function (Davis & Bezprozvanny, 2001; Marder & Prinz, 2003; Turrigiano, 2008). To date these ideas have drawn largely from studies of invertebrate circuits and the vertebrate forebrain. We believe the present results illustrate how synaptic homeostasis may serve autonomic homeostasis, as originally envisioned by Cannon.

Mechanisms that tightly regulate behaviour of a system often include opposing processes that allow for growth and decay, with one serving as driver and the other as feedback. It is now evident that opposing forces of this type operate on gK_M in sympathetic B neurons through M_1-muscarinic receptors that suppress the conductance and action potentials that enhance it. Both mechanisms are driven by preganglionic cholinergic synapses. The ability of these opposing mechanisms to maintain a stable set point for ganglionic gain will thus depend on the interplay between integration of fast EPSPs, muscarinic excitation and postsynaptic firing.

Expression of homeostatic I_M regulation in secretomotor, but not vasomotor neurons, suggests two different roles in ganglionic integration. In the first, ganglionic integration in the secretomotor system maintains synaptic gain at a relatively constant set point for different levels of preganglionic activity. In the second, I_M is insensitive to activity in the vasomotor system, thus allowing its suppression by peptidergic transmission (Jan *et al.* 1980; Adams *et al.* 1982*b*) to increase synaptic gain in proportion to preganglionic activity. The resulting variable gain generated in vasomotor ganglionic synapses could thereby contribute to the overall gain of baroreceptor and other cardiovascular reflexes.

References

Adams PR & Brown DA (1982). Synaptic inhibition of the M-current: slow excitatory post-synaptic potential mechanism in bullfrog sympathetic neurones. *J Physiol* **332**, 263–272.

Adams PR, Brown DA & Constanti A (1982*a*). M-currents and other potassium currents in bullfrog sympathetic neurones. *J Physiol* **330**, 537–572.

Adams PR, Brown DA & Constanti A (1982*b*). Pharmacological inhibition of the M-current. *J Physiol* **332**, 223–262.

Bratton B, Davies P, Jänig W & McAllen R (2009). Ganglionic processing in vasomotor pathways. *Auton Neurosci* **149**, 120.

Brown DA & Adams PR (1980). Muscarinic suppression of a novel voltage-sensitive K^+ current in a vertebrate neurone. *Nature* **283**, 673–676.

Brown DA, Gahwiler BH, Griffith WH & Halliwell JV (1990). Membrane currents in hippocampal neurons. *Prog Brain Res* **83**, 141–160.

Brown DA & Selyanko AA (1985). Membrane currents underlying the cholinergic slow excitatory post-synaptic potential in the rat sympathetic ganglion. *J Physiol* **365**, 365–387.

Constanti A & Brown DA (1981). M-Currents in voltage-clamped mammalian sympathetic neurones. *Neurosci Lett* **24**, 289–294.

Constanti A & Galvan M (1983). M-current in voltage-clamped olfactory cortex neurones. *Neurosci Lett* **39**, 65–70.

Davis GW & Bezprozvanny I (2001). Maintaining the stability of neural function: a homeostatic hypothesis. *Annu Rev Physiol* **63**, 847–869.

Delmas P & Brown DA (2005). Pathways modulating neural KCNQ/M (Kv7) potassium channels. *Nat Rev Neurosci* **6**, 850–862.

Dodd J & Horn JP (1983). A reclassification of B and C neurones in the ninth and tenth paravertebral sympathetic ganglia of the bullfrog. *J Physiol* **334**, 255–269.

Drummond GB (2009). Reporting ethical matters in *The Journal of Physiology*: standards and advice. *J Physiol* **587**, 713–719.

Ford CP, Stemkowski PL, Light PE & Smith PA (2003). Experiments to test the role of phosphatidylinositol 4,5-bisphosphate in neurotransmitter-induced M-channel closure in bullfrog sympathetic neurons. *J Neurosci* **23**, 4931–4941.

Gamper N & Shapiro MS (2003). Calmodulin mediates Ca^{2+}-dependent modulation of M-type K^+ channels. *J Gen Physiol* **122**, 17–31.

Gamper N, Reznikov V, Yamada Y, Yang J & Shapiro MS (2004). Phosphatidylinositol [correction] 4,5-bisphosphate signals underlie receptor-specific Gq/11-mediated modulation of N-type Ca^{2+} channels. *J Neurosci* **24**, 10980–10992.

Halliwell JV (1986). M-current in human neocortical neurones. *Neurosci Lett* **67**, 1–6.

Hernandez CC, Zaika O & Shapiro MS (2008*a*). A carboxy-terminal inter-helix linker as the site of phosphatidylinositol 4,5-bisphosphate action on Kv7 (M-type) K^+ channels. *J Gen Physiol* **132**, 361–381.

Hernandez CC, Zaika O, Tolstykh GP & Shapiro MS (2008*b*). Regulation of neural KCNQ channels: signalling pathways, structural motifs and functional implications. *J Physiol* **586**, 1811–1821.

Ivanoff AY & Smith PA (1995). *In vivo* activity of B- and C-neurones in the paravertebral sympathetic ganglia of the bullfrog. *J Physiol* **485**, 797–815.

Jan YN, Jan LY & Kuffler SW (1980). Further evidence for peptidergic transmission in sympathetic ganglia. *Proc Natl Acad Sci U S A* **77**, 5008–5012.

Jones SW & Marks TN (1989). Calcium currents in bullfrog sympathetic neurons. I. Activation kinetics and pharmacology. *J Gen Physiol* **94**, 151–167.

Karila P & Horn JP (2000). Secondary nicotinic synapses on sympathetic B neurons and their putative role in ganglionic amplification of activity. *J Neurosci* **20**, 908–918.

Kirkwood A & Lisman JE (1992). Action potentials produce a long-term enhancement of M-current in frog sympathetic ganglion. *Brain Res* **580**, 281–287.

Kuba K, Morita K & Nohmi M (1983). Origin of calcium ions involved in the generation of a slow afterhyperpolarization in bullfrog sympathetic neurones. *Pflugers Arch* **399**, 194–202.

Kullmann PH & Horn JP (2006). Excitatory muscarinic modulation strengthens virtual nicotinic synapses on sympathetic neurons and thereby enhances synaptic gain. *J Neurophysiol* **96**, 3104–3113.

Kullmann PH & Horn JP (2010). Vasomotor sympathetic neurons are more excitable than secretomotor sympathetic neurons in bullfrog paravertebral ganglia. *Auton Neurosci* (in press, doi: 10.1016/j.autneu.2009.12.009).

Kullmann PH, Wheeler DW, Beacom J & Horn JP (2004). Implementation of a fast 16-Bit dynamic clamp using LabVIEW-RT. *J Neurophysiol* **91**, 542–554.

Kurenny DE, Chen H & Smith PA (1994). Effects of muscarine on K^+-channel currents in the C-cells of bullfrog sympathetic ganglion. *Brain Res* **658**, 239–251.

Lawrence JJ, Saraga F, Churchill JF, Statland JM, Travis KE, Skinner FK & McBain CJ (2006). Somatodendritic Kv7/KCNQ/M channels control interspike interval in hippocampal interneurons. *J Neurosci* **26**, 12325–12338.

Marder E & Prinz AA (2003). Current compensation in neuronal homeostasis. *Neuron* **37**, 2–4.

Marrion NV, Smart TG & Brown DA (1987). Membrane currents in adult rat superior cervical ganglia in dissociated tissue culture. *Neurosci Lett* **77**, 55–60.

Marrion NV, Zucker RS, Marsh SJ & Adams PR (1991). Modulation of M-current by intracellular Ca^{2+}. *Neuron* **6**, 533–545.

McCormick DA & Prince DA (1986). Mechanisms of action of acetylcholine in the guinea-pig cerebral cortex in vitro. *J Physiol* **375**, 169–194.

McLachlan EM, Davies PJ, Habler HJ & Jamieson J (1997). On-going and reflex synaptic events in rat superior cervical ganglion cells. *J Physiol* **501**, 165–181.

McLachlan EM, Habler HJ, Jamieson J & Davies PJ (1998). Analysis of the periodicity of synaptic events in neurones in the superior cervical ganglion of anaesthetized rats. *J Physiol* **511**, 461–478.

Pennefather P, Lancaster B, Adams PR & Nicoll RA (1985). Two distinct Ca-dependent K currents in bullfrog sympathetic ganglion cells. *Proc Natl Acad Sci U S A* **82**, 3040–3044.

Romero M, Reboreda A, Sanchez E & Lamas JA (2004). Newly developed blockers of the M-current do not reduce spike frequency adaptation in cultured mouse sympathetic neurons. *Eur J Neurosci* **19**, 2693–2702.

Schobesberger H, Wheeler DW & Horn JP (2000). A model for pleiotropic muscarinic potentiation of fast synaptic transmission. *J Neurophysiol* **83**, 1912–1923.

Shah MM, Migliore M, Valencia I, Cooper EC & Brown DA (2008). Functional significance of axonal Kv7 channels in hippocampal pyramidal neurons. *Proc Natl Acad Sci U S A* **105**, 7869–7874.

Suh BC & Hille B (2002). Recovery from muscarinic modulation of M current channels requires phosphatidylinositol 4,5-bisphosphate synthesis. *Neuron* **35**, 507–520.

Suh BC, Horowitz LF, Hirdes W, Mackie K & Hille B (2004). Regulation of KCNQ2/KCNQ3 current by G protein cycling: the kinetics of receptor-mediated signalling by Gq. *J Gen Physiol* **123**, 663–683.

Suh BC, Inoue T, Meyer T & Hille B (2006). Rapid chemically induced changes of $PtdIns(4,5)P_2$ gate KCNQ ion channels. *Science* **314**, 1454–1457.

Tokimasa T, Shirasaki T & Kuba K (1997). Evidence for the calcium-dependent potentiation of M-current obtained by the ratiometric measurement of the fura-2 fluorescence in bullfrog sympathetic neurons. *Neurosci Lett* **236**, 123–126.

Tokimasa T, Shirasaki T, Yoshida M, Ito M, Tanaka E, Mitsumoto T, Akasu T, Tanaka M, Higashi H & Nakano T (1996). Calcium-dependent potentiation of M-current in bullfrog sympathetic neurons. *Neurosci Lett* **214**, 79–82.

Turrigiano GG (2008). The self-tuning neuron: synaptic scaling of excitatory synapses. *Cell* **135**, 422–435.

Vervaeke K, Gu N, Agdestein C, Hu H & Storm JF (2006). Kv7/KCNQ/M-channels in rat glutamatergic hippocampal axons and their role in regulation of excitability and transmitter release. *J Physiol* **576**, 235–256.

Wang HS, Pan Z, Shi W, Brown BS, Wymore RS, Cohen IS, Dixon JE & McKinnon D (1998). KCNQ2 and KCNQ3 potassium channel subunits: molecular correlates of the M-channel. *Science* **282**, 1890–1893.

Wei AD, Gutman GA, Aldrich R, Chandy KG, Grissmer S & Wulff H (2005). International Union of Pharmacology. LII. Nomenclature and molecular relationships of calcium-activated potassium channels. *Pharmacol Rev* **57**, 463–472.

Wheeler DW, Kullmann PH & Horn JP (2004). Estimating use-dependent synaptic gain in autonomic ganglia by computational simulation and dynamic-clamp analysis. *J Neurophysiol* **92**, 2659–2671.

Winks JS, Hughes S, Filippov AK, Tatulian L, Abogadie FC, Brown DA & Marsh SJ (2005). Relationship between membrane phosphatidylinositol-4,5-bisphosphate and receptor-mediated inhibition of native neuronal M channels. *J Neurosci* **25**, 3400–3413.

Yamada WM, Koch C & Adams PR (1989). Multiple channels and calcium dynamics. In *Methods in Neuronal Modelling*, ed. Koch C & Segev I, pp. 97–133. MIT, Cambridge, MA, USA.

Yu SP (1995). Roles of arachidonic acid, lipoxygenases and phosphatases in calcium-dependent modulation of M-current in bullfrog sympathetic neurons. *J Physiol* **487**, 797–811.

Yu SP, O'Malley DM & Adams PR (1994). Regulation of M current by intracellular calcium in bullfrog sympathetic ganglion neurons. *J Neurosci* **14**, 3487–3499.

Zaika O, Tolstykh GP, Jaffe DB & Shapiro MS (2007). Inositol triphosphate-mediated Ca^{2+} signals direct purinergic P2Y receptor regulation of neuronal ion channels. *J Neurosci* **27**, 8914–8926.

Zhang H, Craciun LC, Mirshahi T, Rohacs T, Lopes CM, Jin T & Logothetis DE (2003). PIP_2 activates KCNQ channels, and its hydrolysis underlies receptor-mediated inhibition of M currents. *Neuron* **37**, 963–975.

Zhao X, Varnai P, Tuymetova G, Balla A, Toth ZE, Oker-Blom C, Roder J, Jeromin A & Balla T (2001). Interaction of neuronal calcium sensor-1 (NCS-1) with phosphatidylinositol 4-kinase β stimulates lipid kinase activity and affects membrane trafficking in COS-7 cells. *J Biol Chem* **276**, 40183–40189.

Author contributions

Both authors contributed to the conception, design, analysis and interpretation of data, and to the writing of the manuscript, and both gave final approval of the version for publication. Most of the experiments were conducted by the first author. The work was carried out at the University of Pittsburgh School of Medicine.

Acknowledgements

This work was supported by NIH grant NS21065.